Multi-Machine Learning Ensemble Regionalization of Hydrological Parameters for Enhancing Flood Prediction in Ungauged Mountainous Catchments

Kai Li, Linmao Guo, Genxu Wang*, Jihui Gao*, Xiangyang Sun, Peng Huang, Jinlong Li, Jiapei Ma, Xinyu Zhang

State Key Laboratory of Hydraulics and Mountain River Engineering, College of Water Resource and Hydropower, Sichuan University, Chengdu, 610000, China

*Corresponding author: Genxu Wang (wanggx@scu.edu.cn) and Jihui Gao (jgao@scu.edu.cn).

Abstract:

Machine learning-based parameter regionalization is an important method for flood prediction in ungauged mountainous catchments. However, single machine learning parameter regionalization often exhibits limitations in prediction accuracy and robustness. Therefore, this study proposes a multi-machine learning ensemble regionalization method that integrates Gradient Boosting Machine (GBM), K-Nearest Neighbors (KNN), and Extremely Randomized Trees (ERT) methods (GBM-KNN-ERT) to regionalize the sensitive parameters of the Topography-Based Subsurface Storm Flow (Top-SSF) model. Validated across 80 mountainous catchments in southwestern China, the GBM-KNN-ERT method demonstrates superior performance with 90% of ungauged catchments achieving the Nash-Sutcliffe Efficiency (NSE) above 0.9, representing a 67.44% improvement over the best single machine learning parameter regionalization. Notably, the GBM-KNN-ERT method shows improved robustness to climate change and changes in the number of donor catchments compared to other regionalization methods. An optimal balance between accuracy and

computational efficiency was achieved using 20-40 high quality donor catchments (NSE greater than 0.85). This study provides systematic evidence that multi-machine learning ensemble can effectively address regionalization challenges in ungauged mountainous regions, offering a reliable tool for water resource management and flood disaster mitigation.

Keywords: Flood forecasting; Regionalization; Ungauged mountainous catchments; Top-SSF model;

Highlights:

1. Proposes a novel multi-machine learning ensemble regionalization method
2. The GBM-KNN-ERT method increases the percentage of catchments with high-accuracy flood predictions (NSE >0.9) to 90%, which is a 67.44% improvement over the best single machine learning method.
3. The GBM-KNN-ERT method exhibits greater stability under climate change.

1. Introduction

Floods in mountainous catchments, encompassing both flash floods and general larger-scale flood events which can be derived from mountainous upland catchments, pose a significant threat to human safety and property, particularly in regions lacking sufficient observational data (Luo et al., 2015; Zhai et al., 2018). While hydrological models like the Topography-Based Subsurface Storm Flow (Top-SSF) model (Li et al., 2024) offer promising simulation capabilities, their application in ungauged catchments is severely limited by the absence of calibration data (Choi et al., 2023; Liu et al., 2018). Effective parameter regionalization methods are therefore essential for transferring hydrological knowledge from gauged to ungauged regions, enabling reliable flood prediction in ungauged mountainous catchment (Garambois et al., 2015; Ragettli et al., 2017; Xu et al., 2018).

Parameter regionalization is a crucial method for flood prediction in ungauged catchments (Arsenault et al., 2022; Guo et al., 2021; Kratzert et al., 2019; Zhang et al., 2020). Compared to purely data-driven methods, parameter regionalization offers enhanced physical interpretability (Nearing et al., 2024; Tang et al., 2023; Zhang et al., 2024). Existing parameter regionalization methods can be broadly classified into three categories: similarity-based, hydrological signatures-based, and regression-based (Arsenault et al., 2019; Wu et al., 2022). Similarity-based methods rely on the assumption that catchments with similar characteristics exhibit similar hydrological responses, considering spatial proximity (Arsenault et al., 2019; Pugliese et al., 2018; Yang et al., 2018) and physical similarity (similar climatic and land cover conditions

have similar hydrological characteristics) (Kanishka et al., 2017; Papageorgaki et al., 2016). Hydrological signature-based methods use hydrological signatures (quantitative metrics that describe statistical or dynamic properties of streamflow) as an intermediate link, establishing relationships first between model parameters and signatures, and then between signatures and catchment descriptors to facilitate parameter transfer (McMillan, 2021; Zhang et al., 2018). Regression-based methods, which directly link hydrological model parameters to catchment descriptors, are widely used due to their simplicity and computational efficiency (Guo et al., 2021; Kratzert et al., 2019; Song et al., 2022; Wu et al., 2022). However, the performance of regression-based methods is frequently constrained by the inherent nonlinearity in the relationships between model parameters and catchment descriptors, coupled with the difficulty in adequately capturing spatial heterogeneity, especially within complex mountainous terrain (Wu et al., 2022).

Recent advances in machine learning offer potential solutions by capturing nonlinear patterns in high-dimensional data. Methods such as Decision Tree (DT), Extremely Randomized Trees (ERT), Gradient Boosting Machine (GBM), K-Nearest Neighbor (KNN), Random Forest (RF), and Support Vector Machines (SVM) have shown promise in parameter regionalization (Golian et al., 2021; Song et al., 2022). However, existing machine learning-based parameter regionalization studies predominantly focus on runoff prediction at coarser temporal scales (daily or monthly) (Li et al., 2022; Wu et al., 2022), leaving a significant gap in high-resolution (hourly or sub-hourly) flood prediction in ungauged mountainous catchments. Moreover, these

studies often rely on single machine learning methods to estimate all hydrological model parameters (Golian et al., 2021; Song et al., 2022; Wu et al., 2022). Given that different machine learning methods operate on distinct principles (Jordan et al., 2015; Zounemat-Kermani et al., 2021) and hydrological model parameters represent diverse hydrological processes (Li et al., 2024), a single machine learning method may not adequately capture the complexity of model parameter estimation (Golian et al., 2021; Wu et al., 2022). Therefore, exploring the multi-machine learning ensemble methods is essential to improve the accuracy of high-resolution flood prediction in ungauged mountainous catchments.

Southwest China's mountainous regions are particularly vulnerable to frequent floods, leading to ecosystem degradation through habitat disruption and biodiversity loss (Gan et al., 2018). The abundance of ungauged catchments in this region poses a significant challenge to reliable flood prediction. To address this critical issue, we systematically evaluate the performance of a novel multi-machine learning ensemble method for regionalizing Top-SSF model parameters across 80 representative catchments (mean area: 1,586 km²) in Southwest China. By assessing ensemble method robustness under climate change and with varying donor catchment configurations, this study aims to significantly enhance flood prediction accuracy in ungauged mountainous catchments, contributing to improved ecosystem resilience, enhanced human safety, and more effective water resource management in the face of escalating climatic pressures.

2. Study area and datasets

2.1. Study area

This study investigated 80 mountainous catchments in Southwestern China, encompassing Sichuan, Yunnan, Guangxi, Guizhou, and Chongqing provinces (Fig. 1). This region exhibits diverse climatic zones, including subtropical monsoon, plateau mountain, and tropical monsoon climates. The selected catchments have an average area of 1,586 km² (ranging from 109 to 6,564km^2), with elevations ranging from 63 to 6,284 meters. Mean annual temperature varies from 15 to 20°C, and annual precipitation ranges from 1,200 to 1,800 mm (Li et al., 2016), with approximately 80% of the annual precipitation occurring during summer and autumn, contributing to frequent flooding events (Cheng et al., 2019). These catchments are situated within a heavily forested region, the second largest in China (Hua et al., 2018), with forest cover ranging from 3% to 92% (mean: 51%), influencing evapotranspiration and runoff generation. Dominant soil types, according to the Genetic Soil Classification of China (Shi et al., 2004), include purple soil (12.20%), yellow soil (11.39%), and red soil (9.52%), each with distinct hydrological properties.

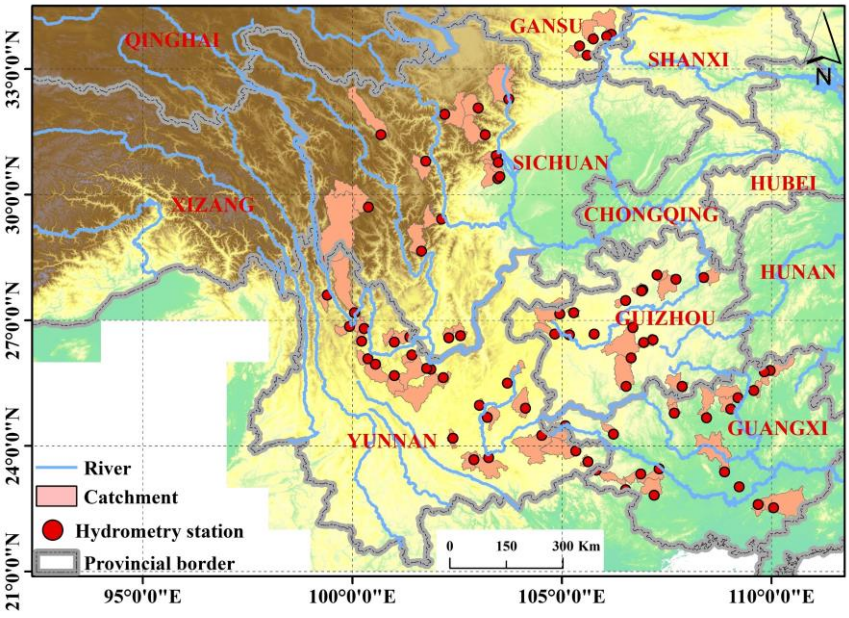

Fig.1. Geographical distribution of the 80 gauged catchments used, with locations of hydrometry station (red points) and major rivers indicated.

2.2. Datasets

Hourly flow data (2015–2018) for 80 mountainous catchments in China were sourced from the Hydrological Bureau of the Ministry of Water Resources, through China's hydrologic yearbooks, encompassing a spectrum of events from flash floods and general floods which can be derived from mountainous upland catchments. Hourly rainfall data (2015–2018) were obtained from ground meteorological stations across China (http://en.weather.com.cn), providing crucial input for hydrological modelling. Additional meteorological variables, including temperature, wind speed, dewpoint temperature, and surface net solar radiation, were obtained from the ERA5 hourly dataset (1940–present) (Hersbach et al., 2023), ensuring comprehensive atmospheric forcing. Relative humidity was estimated using dewpoint temperature. Historical

(1901–2021) and projected future (SSP585, 2022–2100) temperature and precipitation data for China, averaged from the EC-Earth3, GFDL-ESM4, and MRI-ESM2-0 models at 1 km resolution, were obtained from "A Big Earth Data Platform for Three Poles" to assess the impact of climate change (Ding et al., 2020) (http://poles.tpdc.ac.cn). Topographic data, including a 30m resolution Digital Elevation Model (DEM), used for river network and topographic index derivation, were obtained from EARTHDATA (https://search.earthdata.nasa.gov/search). Forest cover data (30m resolution) were sourced from the Global Forest Cover and Forest Change Map (https://www.noda.ac.cn/), providing information on vegetation characteristics. Bulk density (BD) data were derived from the Soil Database of China for Land Surface Modelling (Dai et al., 2013). Soil hydraulic parameters, specifically saturated hydraulic conductivity (Ks_CH) for Clapp and Hornberger functions and the pore-connectivity parameter (L) for van Genuchten and Mualem functions, were acquired from the China Dataset of Soil Hydraulic Parameters Using Pedotransfer Functions for Land Surface Modeling (Shangguan et al., 2013).

Table 1. Model forcing data and catchment descriptors information.

Data type	Name	Unit	Function
Hydro-meteorology	Rainfall	mm	Input for hydrological model
	Flood	m^3/s	Used for model calibration (hourly resolution)
	Temperature	K	Input for hydrological model
	Surface pressure	Pa	
	Dewpoint temperature	K	
	wind speed	m/s	
	Surface net solar radiation	j/m^2	
	Relative humidity	%	
	1 km monthly precipitation (1901-2021)	mm	Multi-year surface average as catchment descriptors
	1 km monthly temperature (1901-2021)	℃	
	1 km monthly temperature (2022-2100, SSP5-8.5, EC-Earth3, GFDL-ESM4, MRI-ESM2-0)	℃	
	1 km monthly precipitation (2022-2100, SSP5-8.5, EC-Earth3, GFDL-ESM4, MRI-ESM2-0)	mm	
Soil characteristics	Soil bulk density (BD)	g/cm^3	Surface average as catchment descriptors
	Pore-connectivity parameter (L) for the van Genuchten and Mualem functions	-	
	Saturated hydraulic conductivity (Ks_CH) of the Clapp and Hornberger Functions	$cm\ d^{-1}$	
Topography	Forest cover (FC)	%	
	DEM	m	
	Topographic index	-	
	Slope	mm^{-1}	
	Catchment area	km^2	

3. Methodology

3.1. Hydrological model

Top-SSF is a semi-distributed hydrological model based on the well-established TOPMODEL framework, which delineates sub-basins based on the topographic index. It retains the key advantages of TOPMODEL, such as its parsimonious structure, physical interpretability, and ease of parameter transfer (Beven et al., 2021; Gao et al., 2018), consists of 15 parameters representing six key hydrological components: canopy interception, infiltration, evapotranspiration, unsaturated zone moisture transport, subsurface storm flow, and flow routing (Li et al., 2024). In the Top-SSF model, flood can be comprised of four components: infiltration-excess overland flow, saturation-excess overland flow, subsurface storm flow, and groundwater discharge.

Infiltration-excess overland flow occurs when the rainfall intensity exceeds the

infiltration capacity. In this study, infiltration is simulated using the Green-Ampt model. When surface ponding occurs, the infiltration rate is determined by solving the Green-Ampt equation iteratively, for which the Newton-Raphson method is employed. The infiltration rate (f_{in}) is given by：

$$f_{in} = -\frac{Ks(CD+F_{satrt})}{Szm(1-e^{(F_{satrt}/Szm)})} \quad (1)$$

where,$f_{in}$is the infiltration rate (m/h)； Ks is surface hydraulic conductivity (m/h)； CD is capillary drive (m); F_{satrt} is the initial cumulative infiltration (m); Szm is the maximum water storage capacity in the unsaturated zone (m).

Saturation excess overland flow occurs at computational cell i when the groundwater table depth, S_i is less than or equal to zero (i.e., $S_i \leq 0$, indicating the water table has reached the surface). It is calculated as:

$$r_{s,i} = max\{Suz_i - max(S_i, 0), 0\} \quad (2)$$

where, $r_{s,i}$ is the depth of saturation excess overland flow generated at cell i (m); Suz_i is the soil water storage in the unsaturated zone, at cell i (m); $S_i$is the groundwater table depth at cell i (m).

The depth of subsurface storm flow generated at computational cell i , $r_{sf,i}$ is given by:

$$r_{sf,i} = q_{sf0}(1 - S_{sf,i}/S_{fmax}) \quad (3)$$

where, $r_{sf,i}$ is the depth of subsurface storm flow at cell i (m); q_{sf0} is initial subsurface storm flow (m); $S_{sf,i}$ is the water storage deficit in the subsurface storm flow zone at cell i (m).

The depth of groundwater discharge is calculated as:

$$r_b = e^{\ln Te-\lambda-\overline{S}_g/Szm} \quad (4)$$

where, r_b is depth of groundwater discharge (m);$lnTe$ is the log of the areal average of $T0$ (m^2/h); is the catchment average topographic index; $\overline{S}_g$ is the catchment average groundwater table depth (m). For the complete set of equations for the Top-SSF model, the reader is referred to the Supplementary Material and (Li et al., 2024).

3.2. Multi-machine learning ensemble method

To improve flood prediction accuracy in ungauged mountainous catchments, we proposed a multi-machine learning ensemble method for regionalizing sensitive parameters of the Top-SSF model. This method leverages the complementary strengths of multi-machine learning methods to estimate model parameters based on catchment descriptors (Fig. 2). The characteristics, strengths, and limitations of each machine learning method are summarized in Table 2. The ensemble method employs a cross-validation procedure to select the best-performing machine learning method for each sensitive parameter. These selections are then integrated into a unified regionalization scheme. By mitigating limitations inherent in single machine learning regionalization, such as model bias and overfitting, and by capturing complex hydrological processes in mountainous catchment, this ensemble method aims to achieve more accurate flood prediction in ungauged catchments.

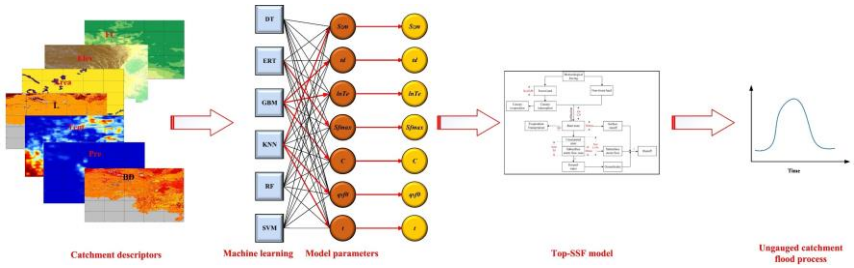

Fig.2. Multi-machine learning ensemble method for regionalization in ungauged mountainous catchments. The red line indicates the machine learning method that yielded the optimal parameter estimates.

Table 2. Seven machine learning model characteristics, advantages and disadvantages.

Machine learning	Characteristic	Advantage	Disadvantages
DT	A single decision tree hierarchically partitions the data space using a tree structure, with internal nodes representing features, branches representing decision rules, and leaf nodes representing class labels.	High interpretability; Minimal data preprocessing.	Unstable; Tends to overfit.
ERT	Construct multiple decision trees with randomly selected feature values and randomly divided nodes (Geurts et al., 2006).	Low overfitting risk; Computational efficiency; Resilient to noise.	Possibility of increased bias; Limited interpretability.
GBM	Construct multiple decision trees. Multiple weak learners are trained iteratively and the loss function is optimised using gradient descent, progressively combined into a robust model through the learning rate (Friedman, 2002).	High accuracy for structured data; Robust to outliers; Minimal data preprocessing.	Limited interpretability; Complex adjustments.
KNN	It is a non-parametric, instance-based supervised learning algorithm. It operates by finding the K nearest data points in the training data to a given data point and making predictions based on these (Wani et al., 2017).	Simple and easy to implement. Learning process is quick.	Sensitivity to noisy and scale of data. Accuracy can be heavily impacted by the choice of K.
RF	A bagging algorithm proposed by Breiman (2001) that uses ensemble learning. Involves training numerous decision trees and aggregating predictions .	Simple and easy to implement; Low computational cost.	Prone to overfitting in noisy regression tasks.
SVM	Identifies hyperplanes in high-dimensional spaces to segregate data. The optimal hyperplane maximizes the margin between it and the nearest data points, termed support vectors (Sain, 1996).	Uses kernel functions to address nonlinear classification issues.	Sensitive to noise

3.3. Parameter regionalization process

The parameter regionalization process comprised four key steps: (1) Top-SSF model calibration and parameter sensitivity analysis; (2) selection of relevant catchment descriptors; (3) establishment of regionalization relationships between sensitive model parameters and catchment descriptors using multi-machine learning ensemble methods; and (4) evaluation of parameter regionalization performance.

3.3.1. Top-SSF model calibration and parameter sensitivity analysis

In this study, the Top-SSF model was employed to simulate hydrological processes. The model was driven by continuous hourly meteorological data, including rainfall, temperature, surface pressure, relative humidity, wind speed, and surface net solar radiation. For each catchment, model parameters were calibrated using two hydrologically independent and representative flood events. A third, distinct flood

event was then used for model validation. The Nash-Sutcliffe Efficiency (NSE) served as the objective function during calibration, with parameter optimization achieved using the Shuffled Complex Evolution (SCE-UA) algorithm (Duan et al., 1994), known for its global convergence and robustness (Dakhlaoui et al., 2012; Qi et al., 2016). Model performance was evaluated using the NSE, the relative error of flood peak flow (Qp), and the absolute error in flood peak occurrence time (Tp), following China's Specification for Hydrological Information Forecast (GB/T 22482-2008). These metrics quantify the model's ability to predict flood dynamics, peak flow, and timing. Following calibration, a sensitivity analysis was conducted to identify and exclude insensitive model parameters (Lenhart et al., 2002), which were then used for regionalization. This approach reduces the dimensionality of the regionalization problem and improves the efficiency of the process.

The sensitivity index (Si) of each hydrological model parameter was determined using the method of Lenhart et al. (2002), which assesses the influence of ±10% changes in parameter values (Eq. 5). Table 3 outlines the sensitivity analysis results for the model parameters across the 80 mountainous catchments. The Si values are categorized as follows (Guo et al., 2022): negligible sensitivity ($|Si| < 0.05$), moderate sensitivity ($0.05 < |Si| < 0.2$), high sensitivity ($0.2 < |Si| < 1.00$), and extremely high sensitivity ($|Si| \geq 1.00$). Based on the sensitivity analyses, seven sensitive model parameters were identified: Szm, $lnTe$, $Sfmax$, C, $qsf0$, t (Table 3).

$$Si = \frac{1}{N}\sum_{t}^{N}\frac{(y_2(t)-y_1(t))/y_0(t)}{2\Delta x/x_0} \quad (5)$$

where $y_0(\mathrm{t})$ is the flood value of the calibrated parameter x_0 at time t; Δx is the

adjusted parameter difference, $\Delta x/x_0$=10%； $y_1(\mathrm{t})$ is the flood value of the calibrated parameter $x_0-\Delta x$ at time t;$y_2(\mathrm{t})$ is the flood value of the calibrated parameter $x_0+\Delta x$ at time t.

Table 3. Top-SSF model main modules and default range of parameters.

Module	Parameter	Definition	Unit	Default range	Sensitivity index
Canopy interception	Sc	Canopy storage capacity	m	0.00~0.01	<0.05
	St	Trunk storage capacity	m	0.00~0.01	<0.05
	Pt	Proportion of rain diverted into stemflow per cover	%	0.00~1.00	<0.05
Evapotranspiration	$Sr0$	Initial root zone storage deficit	m	0.00~0.02	<0.05
	$Srmax$	Maximum root zone storage deficit	m	0.00~2	<0.05
Infiltration	Ks	Surface hydraulic conductivity	m/h	0~0.01	<0.05
	CD	Capillary drive (Morel-Seytoux et al., 1974)	m	0~5	<0.05
Unsaturated zone	$Suz0$	Initial baseflow per unit area	m	0.00~10^{-4}	<0.05
	Szm	Soil maximum water storage capacity	m	0.00~1.00	**0.19**
	td	Unsaturated zone time delay per unit storage deficit	h/m	0~3	**1.07**
	$lnTe$	log of the areal average of T0	m^2/h	-2.00~1.00	**3.4**
Subsurface storm flow zone	$Sfmax$	Maximum subsurface storm flow zone deficit	m	0.00~0.01	**0.16**
	C	Transfer coefficient	m^{-2}/h	0.00~0.1	**0.26**
	$qsf0$	Initial subsurface storm flow per unit area	m	0.00~0.02	**0.18**
Routing	t	Flow routing correction coefficient	-	0.00~5.0	**1.21**

Note, the bolded values in the sensitivity index indicate sensitive model parameters (i.e., |Si|>0.05).

3.3.2. Catchment descriptor selection

To mitigate the effects of multicollinearity on the accuracy and reliability of the parameter regionalization methods, catchment descriptors were screened using the variance inflation factor (VIF) and correlation coefficients. A VIF threshold of less than 10 (VIF < 10) was used to indicate acceptably low multicollinearity (Salmeron et al., 2018). Initial screening identified strong correlations between several descriptor pairs,

notably L with Ks_CH, and Tem with Elev. Furthermore, the VIF values for Ks_CH and Slope were found to exceed 10. Consequently, Ks_CH and Slope were removed from the potential set of descriptors. Following their removal, a re-evaluation of the VIF for the remaining descriptors was conducted. Although a notable correlation exists between Tem and elevation (Elev), their VIF values in the reduced set were both below the threshold of 10. Given the importance of Tem for representing climate impacts and Elev as a key topographic driver, both were retained to preserve potentially valuable information. The final set of seven catchment descriptors selected for regionalization therefore comprised FC, Elev, Area, L, Tem, Pre, and BD. As illustrated in Fig. 3b, the correlations among these final descriptors and the sensitive model parameters are generally low (highest at 0.5), suggesting that the relationships are complex and nonlinear.

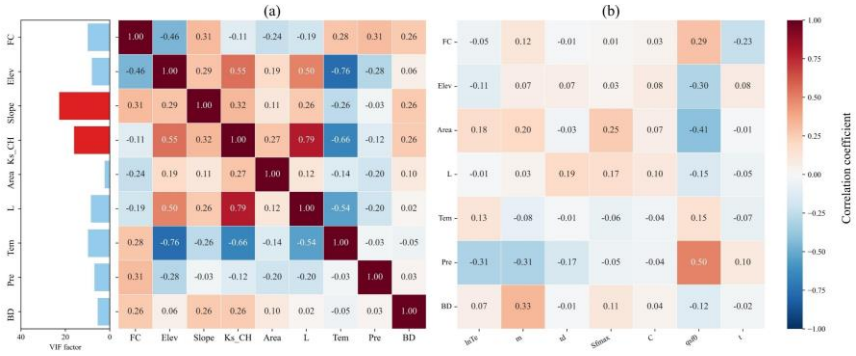

Fig.3. Analysis of catchment descriptor relationships: (a) Correlation coefficients and variance inflation factors (VIF) among all descriptors; (b) Correlation coefficients between sensitive model parameters and descriptors with VIF values below 10.

3.3.3. Parameter regionalization

To simulate ungauged catchment conditions, each of the 80 catchments was iteratively treated as an ungauged catchment, with the remaining 79 catchments serving

277 as donor catchments. A parameter regionalization method was then constructed using
278 the catchment descriptors and sensitive model parameters of the donor catchments to
279 predict the seven sensitive model parameters for the ungauged catchment based on its
280 catchment descriptors. These predicted model parameters were then input into the Top-
281 SSF model to enable flood prediction in ungauged catchments. To ensure robust and
282 generalizable results, K-fold cross-validation (K = 10) was implemented. This involved
283 randomly partitioning the 79 donor catchments into K subsets, using one subset as a
284 test set and the remaining K-1 subsets for method training in each iteration (Jung, 2018).
285 This approach maximizes data utilization and minimizes bias associated with specific
286 data partitioning. Hyperparameter tuning for each machine learning method was
287 performed using RandomizedSearchCV (Bergstra et al., 2012), with the objective of
288 minimizing the difference between predicted and observed parameter values.

289 **3.3.4. Evaluated metrics**

290 The performance of the parameter regionalization methods was evaluated by
291 considering two key aspects. First, the accuracy of the methods in estimating sensitive
292 model parameters was assessed using three metrics: root mean square error (RMSE),
293 standard deviation (STD), and the coefficient of determination (R^2). The R^2 was used
294 to quantify the agreement between estimated and calibrated parameter sets. Second, to
295 evaluate the impact of parameter regionalization on flood prediction. The resulting
296 flood predictions were then evaluated using the NSE, Qp, and Tp metrics.

297 $$NSE = 1 - \frac{\sum_{j=1}^{M}(Q_{obs}(j) - Q_{sim}(j))^2}{\sum_{j=1}^{M}(Q_{obs}(j) - \overline{Q}_{obs})^2} \quad (6)$$

298 $$Q_p = \left| \frac{Q_{obs,p} - Q_{sim,p}}{Q_{obs,p}} \times 100\% \right| \quad (7)$$

$$T_p = \left| T_{obs,p} - T_{sim,p} \right| \quad (8)$$

where $Q_{obs}(j)$ is the observed flow rate (m^3/s); $Q_{sim}(j)$ is the simulated flow rate (m^3/s); $\overline{Q}_{obs}$ is the mean value of the observed flow rate (m^3/s); $Q_{obs,p}$ is the observed flood peak flow (m^3/s); $Q_{sim,p}$ is the simulated flood peak flow (m^3/s); $T_{obs,p}$ is the observed flood peak occurrence time (h); and $T_{sim,p}$ is the simulated flood peak occurrence time (h).

$$RMSE = \sqrt{\frac{1}{N}\sum_{i=1}^{n}(X_i - Y_i)^2} \quad (9)$$

$$STD = \sqrt{\frac{1}{N-1}\sum_{i=1}^{N}(Y_i - \overline{Y})^2} \quad (10)$$

$$R^2 = \frac{[\sum_{i=1}^{n}(X_i - \bar{X})(Y_i - \bar{Y})]^2}{\sum_{i=1}^{n}(X_i - \bar{X})^2 \sum_{i=1}^{n}(Y_i - \bar{Y})^2} \quad (11)$$

where X_i is the Top-SSF calibration model parameter value; Y_i is the model parameter estimated value using the parameter regionalization method; $\overline{X}$ and $\overline{Y}$ are the mean values of X_i and Y_i; N is the sample size equal to 80.

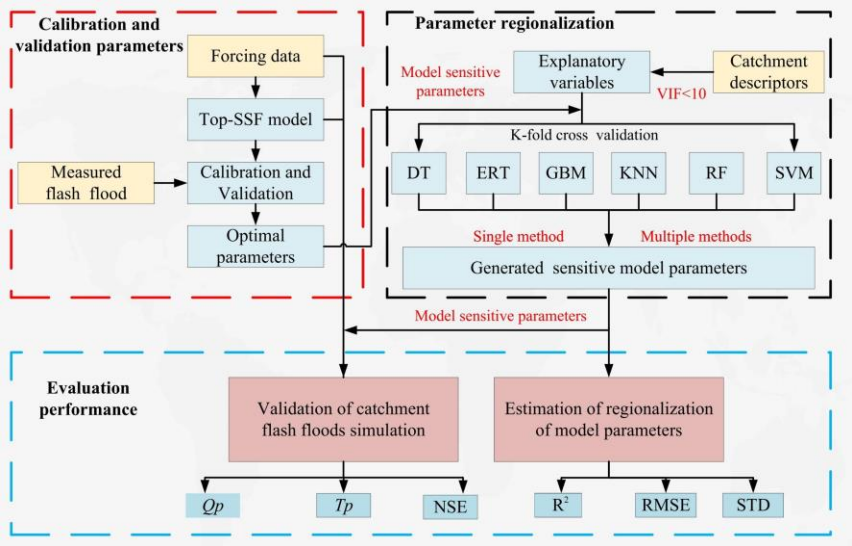

Fig.4. Flowchart illustrating the parameter calibration, validation, and regionalization workflow. Abbreviations: Top-SSF (Topography-Based Subsurface Storm Flow hydrological model), DT (Decision Tree), ERT (Extremely Randomized Trees), GBM (Gradient Boosting Machine), KNN (K-Nearest Neighbor), RF (Random Forest), SVM (Support Vector Machine), NSE (Nash-Sutcliffe efficiency), R^2 (Coefficient of Determination), Qp (The relative error of flood peak flow), Tp (The absolute error in flood peak occurrence time), VIF (Variance inflation factor), RMSE (Root mean square error), STD (Standard deviation).

4. Result

4.1. Model performance

The Top-SSF model demonstrated good flood simulation performance across the 80 gauged catchments, as quantified by NSE, Qp, and Tp. During the calibration period, 50% of the catchments achieved NSE values exceeding 0.78 (Fig. 5a), the median Qp value was below 10% (Fig. 5b), and the median Tp value was within 2 hours (Fig. 5c). The average NSE value was approximately 0.8, with a maximum of 0.96. The majority of Qp values were around 8%, and the majority of Tp values were below 2 hours. During the validation period, the median NSE value was 0.76 (Fig. 5a), the median Qp

value was below 10% (Fig. 5b), and the median Tp value was within 4 hours (Fig.5c). The hydrological response times for the 80 catchments were approximated as the time from precipitation peak to flood peak. The estimated range is from 1 to 26 hours. This diversity is indicative of the comprehensive nature of the study, which encompasses both rapid flash floods in smaller basins and more general floods in larger, mountainous catchments (mean area: 1,586 km²). For catchments with longer response times, a median error of 2-4 hours remains operationally valuable for providing sufficient flood warning lead time. It is noteworthy that the median Tp during the calibration period (within 2 hours) satisfied China's Specification for Hydrological Information Forecast (GB/T 22482-2008) stringent requirements for high-quality forecasts.

Model performance also exhibited some dependence on catchment characteristics. For instance, NSE generally improved with increasing forest cover (Fig. 6a), potentially due to the model's explicit representation of forest canopy interception and subsurface storm flow generation mechanisms. The relationship between NSE, Qp, Tp and elevation was more complex, suggesting a nonlinear influence of elevation on model performance (Fig. 6 a-c). The demonstrated robust performance of the Top-SSF model provides a strong foundation for its application in subsequent parameter regionalization analyses.

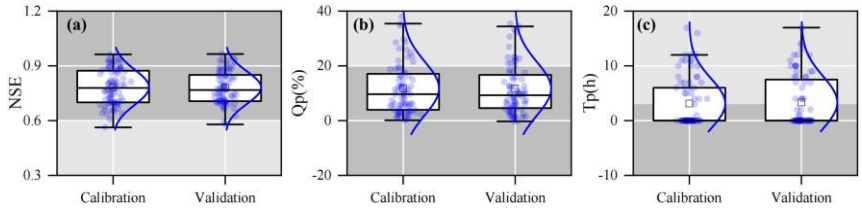

Fig. 5. Boxplots of (a) NSE, (b) Qp, and (c) Tp during the calibration and validation periods for 80 gauged catchments. The box represents the interquartile range, with the middle line indicating the median (50th percentile). The whiskers represent the minimum and maximum values. "□" represents the mean value. Dark grey indicates the range of flood prediction criteria (i.e., NSE> 0.75, Qp< 20%, and Tp < 2 hours).

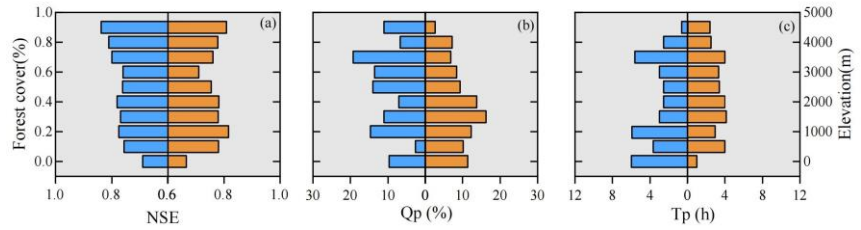

Fig.6. Influence of environmental factors on Top-SSF model performance in flood simulation. The graphs illustrate the relationship between model evaluation metrics and forest cover (left) and elevation (right).

4.2. Results of parameter regionalization

4.2.1. Comparison of sensitive model parameter estimates

The six single machine learning regionalization methods exhibited varying performance in estimating sensitive model parameters (Fig. 7), likely due to differences in catchment descriptor characteristics and the underlying principles of each method. Their hyperparameter results are presented in Tables S1–S6 of the supplementary material. The GBM demonstrated the highest accuracy in estimating Szm, td, and C (R^2 = 0.90, 0.86, and 0.87, respectively,), with its estimates also exhibiting a STD that closely matched the distribution of the calibrated parameter values. KNN provided the most accurate estimates for $lnTe$, $qsf0$, and t (R^2 = 0.87, 0.89, and 0.90, respectively), also with STD closely resembling the calibrated parameter distributions. ERT

performed best in estimating $Sfmax$ (R^2 = 0.87), but its performance was generally poorer for other parameters. DT, SVM, and RF methods generally showed lower performance across all sensitive model parameters. These differences in performance highlight the potential benefits of multi-machine learning ensemble methods for improving flood prediction in ungauged mountainous catchments.

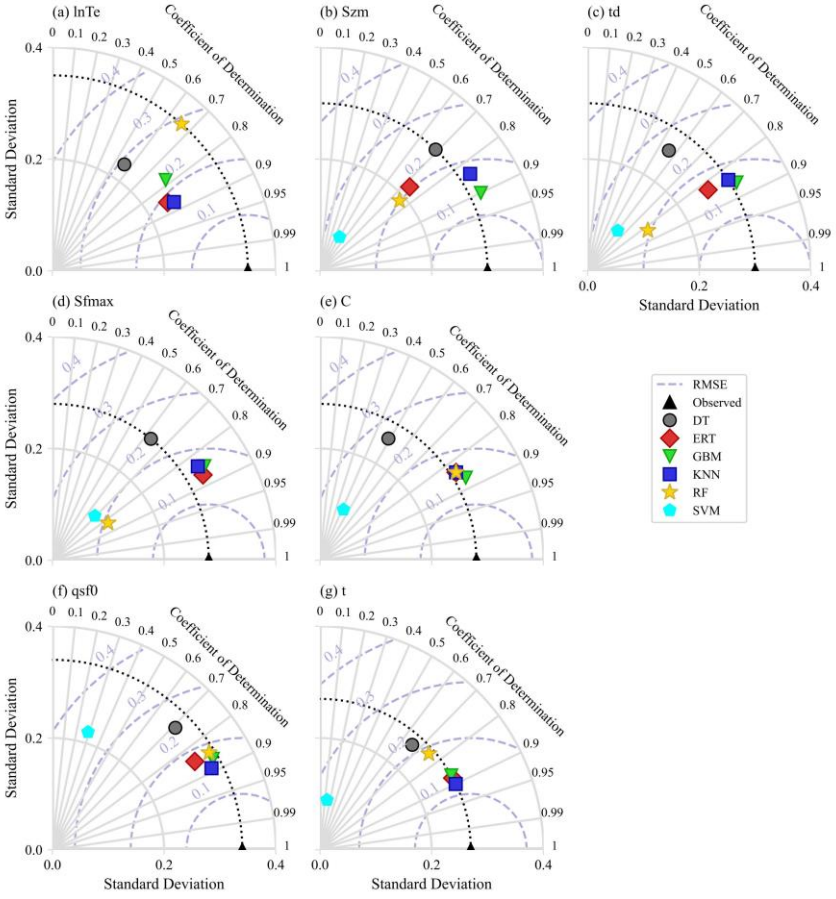

Fig.7. Performance of parameter regionalization methods assessed using Taylor diagrams. The diagrams show the accuracy of sensitive model parameter estimates, with the coefficient of determination (R^2) indicated by the radial axis, standard deviation (STD) by the horizontal and vertical axes, root mean square error (RMSE) by the grey-blue dotted lines, and the standard deviation of observations by the black dotted line."

4.2.2. Comparison of flood forecasting results

The flood prediction performance of the Top-SSF model, integrated with different parameter regionalization methods, was compared across 80 mountainous catchments in southwestern China. The methods included single machine learning methods and a multi-machine learning ensemble method (GBM-KNN-ERT), where GBM estimated Szm, td, and C; KNN estimated $lnTe$, $qsf0$, and t; and ERT estimated $Sfmax$. The performance of these parameter regionalization methods was then evaluated against the performance of the Top-SSF model using calibrated parameters. Among the single machine learning methods, GBM performed best, with 60 catchments achieving a positive NSE (NSE > 0, Fig. 8d). Critically, for high-accuracy predictions (NSE > 0.9), GBM succeeded in 43 catchments (54%), also showing strong performance with Qp less than 5% and Tp less than 1 hour in most cases (Fig. 8a-c). The GBM-KNN-ERT ensemble method yielded even better results. It increased the number of catchments with positive NSE to 75 (Fig. 8d). More impressively, the ensemble method achieved exceptional performance (NSE > 0.9) in 72 catchments (90%). This represents a 67.44% increase in the number of high-accuracy predictions compared to the best single method (GBM). Furthermore, the ensemble method Qp values were more concentrated around zero, and 90% of catchments maintained near-zero Tp values. These results demonstrate the superior potential of multi-machine learning ensembles for improving flood prediction in ungauged catchments.

To further illustrate these performance differences visually, Fig. 8 (e, f, and g) presents hydrographs from three randomly selected flood events. These events

represent cases where the calibrated Top-SSF model itself achieved high (NSE=0.91), medium (NSE=0.76), and low (NSE=0.55) performance, respectively. A key insight from these plots is that the Top-SSF simulation (solid black line) is the performance benchmark for the regionalization methods. Although the models aim to approximate measured floods, their performance is ultimately limited by the accuracy of the Top-SSF model structure and its optimized parameters.

The hydrographs show how the GBM-KNN-ERT ensemble achieves superior performance by leveraging the complementary strengths of its component methods. For instance, in the high-performance case (Fig. 8e), the GBM and KNN methods capture the overall shape well, but the ERT simulation provides a more precise estimation of the primary flood peak. The final ensemble successfully integrates this peak accuracy, resulting in the highest overall performance. Similarly, Fig. 8f shows that the ensemble moderates the slow initial rise characteristic of the KNN method, leading to a more realistic rising limb. The ensemble method ability to balance competing errors is most evident in the low-performance case (Fig. 8g). During the recession phase, the ensemble method averages the high bias of the ERT method with the low bias of the GBM and KNN methods, producing a hydrograph that more closely resembles the benchmark simulation than any single method could. This synergy demonstrates that the ensemble method superior performance is a direct result of its ability to integrate the specific, complementary strengths of each single method across different parts of the hydrological process.

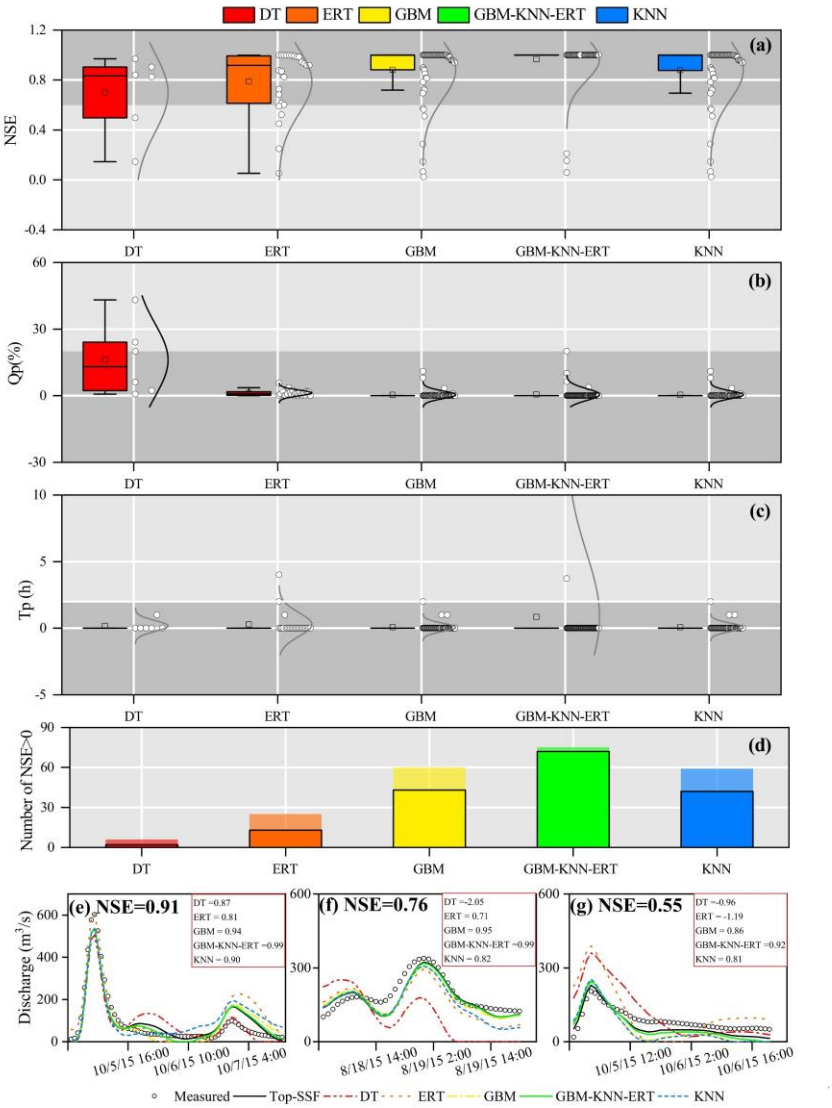

Fig.8. Evaluation of flood prediction performance for different parameter regionalization methods. (a-c) show the distributions of Nash-Sutcliffe Efficiency (NSE), relative peak flow error (Qp), and peak time error (Tp) across all 80 catchments, with shaded regions indicating where flood prediction standards were met (NSE > 0.75, Qp < 20%, and Tp < 2 hours). (d) shows the number of catchments with NSE > 0 and the black border indicates the number of catchments with NSE > 0.9. (e-g) present example hydrographs comparing the simulated flood from each regionalization method against measured flood flow and the calibrated Top-SSF model benchmark for catchments where the benchmark model performance was (e) high (NSE=0.91), (f) medium (NSE=0.76), and (g) low (NSE=0.55).

5. Discussion

5.1. Reliability of multi-machine learning ensemble in parameter regionalization

In this study, the GBM-KNN-ERT method demonstrated superior regionalization performance, highlighting the potential of ensemble methods for improving hydrological predictions in ungauged mountainous catchments. The success of the ensemble is rooted in the distinct learning mechanisms and behaviors of its individual components, which were revealed during hyperparameter optimization.

The GBM method exhibited distinct parameter-specific sensitivities to hyperparameters (Fig. 9a-c). For parameter C, the negative correlation between R^2 and n_estimators (>300 trees) indicates overfitting risks when modeling complex rainfall-runoff interactions in heterogeneous mountainous terrain (Fig. 9a). This aligns with previous findings emphasizing the need for complexity control in hydrological generalization (Schoups et al., 2008). Conversely, the improved R^2 for parameter td with increased n_estimators highlights the capacity of ensemble learning to capture complex, nonlinear relationships between catchment descriptors and hydrological parameters (Hastie et al., 2009). The contrasting optimal max_depth of 10 layers for parameter C, compared to shallower optimal depths (4 layers) for Szm and td, suggests that parameters governing more complex hydrological processes in mountainous catchments may require deeper decision trees to effectively capture the interactions between climate, topography, and soil properties (Wainwright et al., 2013).

KNN performance exhibited pronounced sensitivity to neighbourhood size (n_neighbors) and distance metric (p), highlighting the spatial heterogeneity of

458 catchment descriptors. For parameters $lnTe$ and $qsf0$, optimal performance was
459 observed at n_neighbors =30 (Fig. 9d), aligns with the hypothesis that meaningful
460 hydrological similarities can emerge even in topographically complex mountainous
461 regions when considered at broader spatial scales (Li et al., 2022). Conversely,
462 parameter t achieved peak accuracy at n_neighbors=5, suggesting that localized, short-
463 term weather events and fine-scale topographic similarities in adjacent mountainous
464 areas can significantly influence local runoff processes (Garambois et al., 2015).The
465 Manhattan distance metric (p=1) outperformed Euclidean distance across all
466 parameters (Fig. 9e). This superiority stems from its ability to mitigate the curse of
467 dimensionality (Bellman, 1961) in high-dimensional datasets, a common characteristic
468 of mountainous catchments. In such datasets, sparse data distributions and the presence
469 of mixed variable types (e.g., topographic indices, land cover) can significantly degrade
470 the discriminative power of Euclidean distance (Rockström et al., 2023). The
471 robustness of the Manhattan distance arises from its axis-aligned sensitivity, which
472 provides a more effective means of handling feature scaling and integrating catchment
473 descriptors compared to the radial symmetry of Euclidean distance.
474 ERT performance was maximized at max_features = 0.1 (Fig. 9f). By restricting
475 the random sampling of features during node splits (using only 10% of the features),
476 both the diversity of the trees was enhanced and the effects of multicollinearity between
477 topographic and soil attributes were reduced. This finding aligns with the theory
478 proposed by Geurts et al. (2006), which suggests that random feature selection can
479 significantly improve model generalization, a particularly important consideration in

ungauged mountainous catchments characterized by high levels of inter-correlation among predictor variables.

These distinct sensitivities and learning mechanisms form the scientific basis for the superiority of the GBM-KNN-ERT method. As shown in Section 4.2, no single machine learning method is universally optimal for all hydrological model parameters. Instead, the ensemble method effectively allocates each parameter to the model best suited for its regionalization. Specifically, GBM, with its capacity for modeling complex interactions, proved optimal for integrated parameters like Szm and td. In contrast, the instance-based KNN was superior for parameters like $lnTe$, which are governed by physical similarity and spatial coherence. Finally, the highly randomized nature of ERT provided the necessary robustness to model the noisy relationship associated with the $Sfmax$ .This synergistic combination, where each model contributes its unique strength, results in a final regionalization method that is more accurate and physically plausible than any individual method operating in isolation.

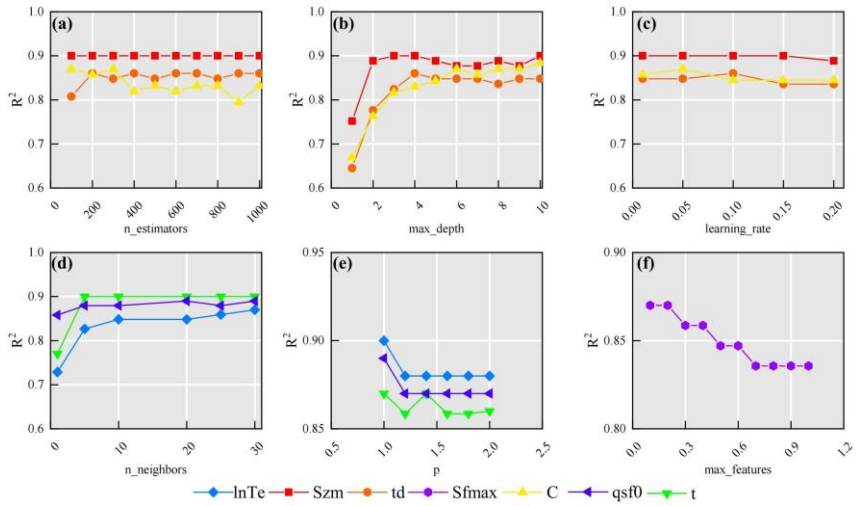

Fig.9. Sensitivity of parameter estimation performance to key hyperparameters in (a-c) GBM, (d-e) KNN method, and (f) ERT. (a) n_estimators (number of decision trees in GBM), (b) max_depth (maximum depth of decision trees in GBM), (c) learning rate (GBM), (d) n_neighbors (number of neighbors in KNN), (e) p-value of Minkowski distance (KNN; p=1: Manhattan distance, p=2: Euclidean distance), and (f) max_features (ERT).

5.2. Combining multiple machine learning methods for parameter regionalization

Machine learning methods exhibit distinct strengths in hydrological parameter estimation due to fundamental differences in data processing mechanisms, pattern recognition strategies, and prediction generation (Bishop et al., 2006). This suggests that multi-machine learning ensemble methods have the potential to synergistically integrate advantages while effectively compensating for individual limitations, leading to more robust and accurate parameter estimates. As demonstrated in Fig. 10, the GBM-KNN-ERT method achieved notable improvements over any single machine learning method, particularly for sensitive parameters $lnTe$, $Sfmax$, $qsf0$ and t, with R^2 increases ranging from 0.02 to 0.03 compared to the best-performing GBM method (Fig.10e).

513 Interestingly, a comparison of GBM4-KNN3 (where $Sfmax$ is estimated by GBM)
514 and GBM3-KNN4 (where $Sfmax$ is estimated by KNN) revealed critical insights into
515 model parameter compatibility. Despite both achieving an identical R^2 of 0.85 for the
516 estimation of $Sfmax$, GBM4-KNN3 exhibited superior flood prediction performance,
517 with 72 catchments achieving NSE > 0 compared to only 68 catchments for GBM3-
518 KNN4. This suggests that GBM possesses an enhanced capability to resolve the
519 complex coupling between soil moisture dynamics and topography, leading to more
520 physically plausible representation of subsurface storm flow processes (Gupta et al.,
521 2023). The wider distribution of flood prediction performance observed for GBM3-
522 KNN4 (Fig. 10 a–c) further suggests that uncertainties introduced by KNN in the
523 estimation of $Sfmax$ may propagate nonlinearly during flood simulations, potentially
524 amplifying errors. This observation aligns with theoretical expectations that distance-
525 based methods may tend to oversmooth critical thresholds or sharp transitions in
526 heterogeneous environments, leading to a less accurate representation of hydrological
527 responses (Bellman, 1961).

528 Furthermore, an important consideration in adopting ensemble methods is the
529 trade-off between predictive accuracy and computational efficiency. To evaluate this
530 trade-off, the model training times for various parameter regionalization methods were
531 compared, and the results are summarized in Table 4. The analysis shows that the
532 proposed GBM-KNN-ERT ensemble, while providing the highest predictive accuracy,
533 required a total training time of 102.8 s. This is moderately higher than the best-
534 performing single model, GBM (57.6 s), and other simpler ensemble methods like

GBM4-KNN3 (36.1 s). The increased computational time for the GBM-KNN-ERT method is primarily attributed to the inclusion of the ERT method for estimating the $Sfmax$, which is inherently more computationally intensive than GBM or KNN.

However, it is crucial to contextualize this computational cost for operational use. The process of training a regionalization method is an offline task, performed once to establish the stable relationships between catchment descriptors and model parameters. This one-time investment is not a constraint on real-time flood forecasting, as once the method is trained, parameter estimation for a new ungauged catchment is nearly instantaneous. For the reported computational times, all model training and simulations were performed on a workstation equipped with an Intel(R) Core (TM) i9-10900K CPU @ 3.70GHz, 32.0 GB of RAM, and an NVIDIA Quadro P1000 (4 GB) GPU, running on a 64-bit Windows operating system with Python 3.9. Given this context, the modest increase in one-time training cost is a justifiable investment for the significant improvements achieved in flood prediction accuracy, model robustness, and stability. Therefore, for applications in water resource management and flood risk assessment where high accuracy is paramount, the GBM-KNN-ERT method strikes an optimal and practical balance between computational efficiency and predictive performance.

批注 [L1]: Comment#1

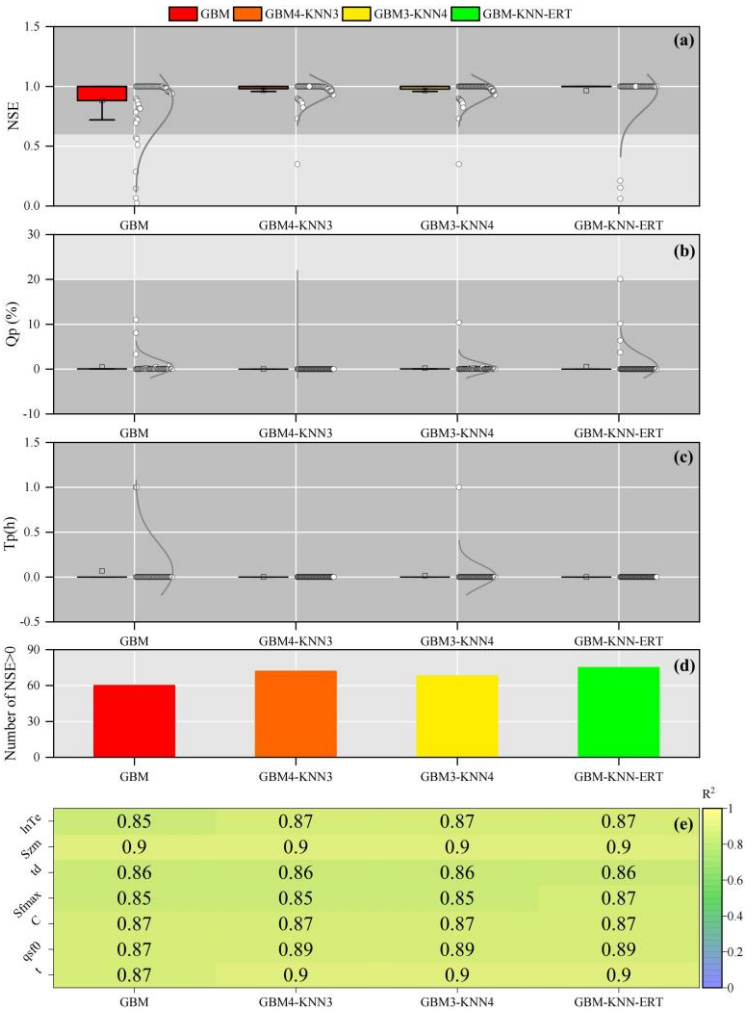

Fig.10. Assessment of combined machine learning methods for improved parameter regionalization in ungauged mountainous catchments. Performance is evaluated against the GBM method, showing (a) NSE, (b) Qp, (c) Tp, (d) Number of catchments with NSE > 0, and (e) the difference in R^2.

Table 4. Running time (s) for different parameter regionalization methods

	GBM	GBM4-KNN3	GBM3-KNN4	GBM-KNN-ERT	KNN	ERT
$lnTe$	11.3	3.4	3.4	3.7	3.6	74.4
Szm	7.8	7.5	7.7	7.8	0.6	76.7
td	8.2	8.1	8.0	8.5	0.6	74.7
$Sfmax$	7.7	8.2	0.6	73.6	0.5	74.9
C	7.8	7.7	7.7	8.0	0.6	74.9
$qsf0$	7.4	0.6	0.6	0.6	0.6	76.3
t	7.4	0.6	0.6	0.6	0.5	75.3
Sum	57.6	36.1	28.6	102.8	7.0	527.2

5.3. The influence of donor catchment quantity on machine-learning parameter regionalization

The number of donor catchments used in machine learning-based parameter regionalization methods is a critical factor influencing the accuracy and robustness of hydrological predictions in ungauged catchments (Gauch et al., 2021; Song et al., 2022; Zhang et al., 2022). This study investigated the influence of donor catchment quantity (ranging from 20 to 80) on the flood prediction performance of the two best-performing parameter regionalization methods (GBM4-KNN3 and GBM-KNN-ERT) across the 80 mountainous catchments (Fig.11). It is important to clarify that the following analysis is not a method for selecting donor catchments based on physical similarity—a task handled by the machine learning methods itself when it learns the relationships between catchment descriptors and model parameters. Instead, this experiment serves as a sensitivity analysis to understand how the regionalization performance is affected by the overall quantity and quality of the available training data.

To systematically investigate the performance influence of donor catchment quantity on parameter regionalization, two distinct sampling strategies were employed across the 80 mountainous catchments. In Mode 1 (selection of donor catchments based on decreasing NSE), which was designed to test the impact of data quality, a non-monotonic relationship was observed. For both methods, regionalization performance peaked with 20-40 donor catchments and then declined, particularly for the GBM4-KNN3 method (Fig. 11a-c). This performance degradation is not due to increasing catchment dissimilarity, but rather to the introduction of lower-quality training data. As the donor pool expands beyond the best-performing catchments, it begins to include

catchments where the Top-SSF model calibration itself was less successful (i.e., lower NSE values). These lower-performance samples may introduce noise and less reliable parameter-descriptor relationships, which can mislead the training process (Gauch et al., 2021; Zhang et al., 2022). Notably, the GBM-KNN-ERT method demonstrated greater resilience to this degradation. Its performance, while also peaking early, did not degrade as sharply and instead tended to stabilize after the inclusion of approximately 70 catchments. This suggests that the more complex ensemble structure has a superior ability to suppress noise and generalize from a dataset containing a mix of high- and low-quality examples, highlighting its enhanced robustness. In contrast, Mode 2 (random selection of donor catchments) demonstrated a consistent improvement in regionalization performance for both NSE and Tp as the number of donor catchments increased (Fig. 11d-f). However, while the average performance improves with data quantity, it is important to acknowledge that this trend relies on the random samples being generally representative; a poorly chosen random set could still reduce generalizability. Notably, under both modes, the GBM-KNN-ERT method consistently exhibited significantly greater performance stability compared to the alternative ensemble, GBM4-KNN3. This enhanced robustness likely arises from its more effective suppression of data heterogeneity and noise interference, indicating that more complex ensemble methods possess a greater capacity to balance the benefits of increased data quantity with the potential drawbacks of reduced data quality.

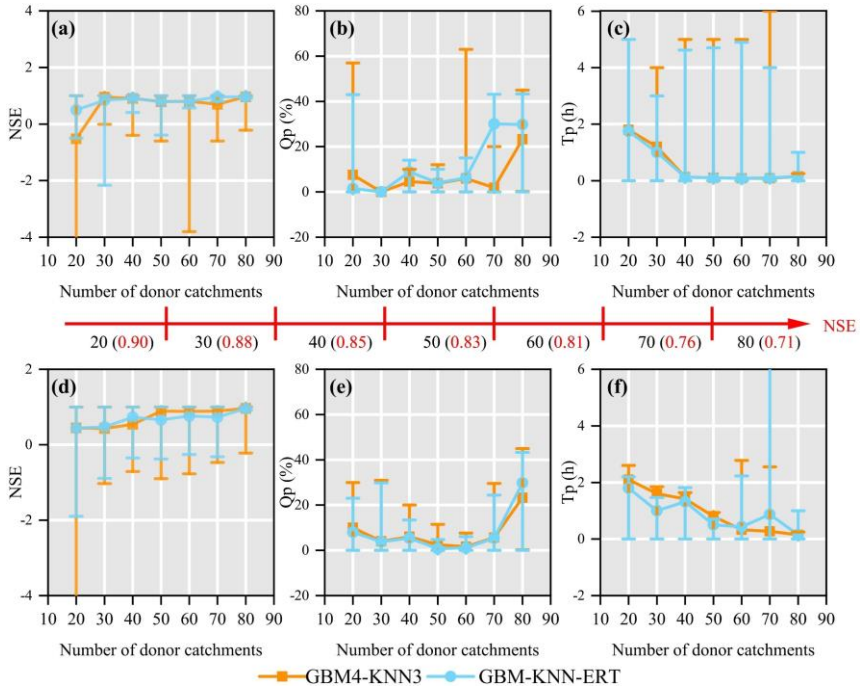

Fig. 11. Performance comparison of two donor catchment selection methods for parameter regionalization as a function of donor catchment quantity. Mode1 (a-c) selects donor catchments in order of decreasing NSE, while Mode 2 (d-f) selects them randomly. Flood prediction accuracy is assessed using NSE, Qp, and Tp. Error bars represent the full range (minimum to maximum) of the performance metrics.

5.4. The impact of climate change on parameter regionalization methods

The hydrological cycle within catchments is fundamentally governed by complex interactions between climate and environmental factors. The Intergovernmental Panel on Climate Change (IPCC) has consistently documented a continuous and accelerating transition in global climatic patterns, characterized by increased variability and extreme events (Pachauri et al., 2014). Consequently, future flood predictions derived from parameter regionalization methods are expected to exhibit increased uncertainty and variability, highlighting the substantial influence of climate change on the reliability and precision of flood predictions in ungauged mountainous catchments (Yang et al.,

2019). Therefore, a sensitivity analysis was designed to evaluate the robustness of the trained regionalization models when confronted with climatic conditions outside their original training range.

To quantitatively assess the impact of climate change, an experiment was devised where this impact was primarily reflected through changes in two key catchment descriptors: Tem and Pre. For the historical period, these descriptors represent the multi-year averages over 1901–2021, while for the future period, they represent the projected multi-year averages over 2022–2100 under the SSP5-8.5 scenario. The regionalization methods (GBM4-KNN3 and GBM-KNN-ERT), which were trained exclusively using historical data, were then applied under these future conditions. Crucially, the method structures and hyperparameters remained fixed, and no retraining was performed; only the historical Tem and Pre values were replaced with their future projections. This approach allows the response of the established historical relationships to new, out-of-sample climatic inputs to be tested. The simulated peak discharges for this analysis were derived from the same three flood events used in the calibration and validation of the Top-SSF model. This experimental design is critical as it isolates the impact of the changed model parameters from the compounding effect of a different future rainfall event. Consequently, any observed change in the simulated flood peak is attributable solely to the sensitivity of the regionalization method to the shift in climatic descriptors. Cumulative distribution functions (CDFs) were then employed to illustrate the discrepancies between the parameter regionalization simulations and the reference simulations (derived from calibrated model parameters) across the historical and

638 projected future periods for the 80 catchments (Fig.12).

639 A comparative analysis of Fig. 12a and 12b reveals a clear amplification of the
640 absolute differences in predicted flood peaks (quantified as the error in runoff modulus)
641 between the two parameter regionalization methods and the reference Top-SSF model
642 simulations during the transition from the historical period to the projected future period.
643 Specifically, the maximum error in runoff modulus for the GBM4-KNN3 method
644 increased by 68.46 $m^3 s^{-1} km^{-2}$ from the historical period to the future period, while the
645 increase for the GBM-KNN-ERT method was a smaller 56.65 $m^3 s^{-1} km^{-2}$. These results
646 underscore that parameter regionalization methods are inherently sensitive to changing
647 climatic forcing. However, they also provide compelling evidence that the GBM-KNN-
648 ERT method exhibits superior stability and resilience under climate change,
649 demonstrating its potential for more reliable long-term flood risk assessment in
650 ungauged mountainous regions.

651 Exploring the effects of climate change on parameter regionalization methods
652 provides valuable insights for advancing flood prediction research in prediction in
653 ungauged basins. The enhanced stability demonstrated by the GBM-KNN-ERT
654 ensemble offers a promising direction for developing robust regionalization methods
655 capable of navigating the challenges of a non-stationary climate.

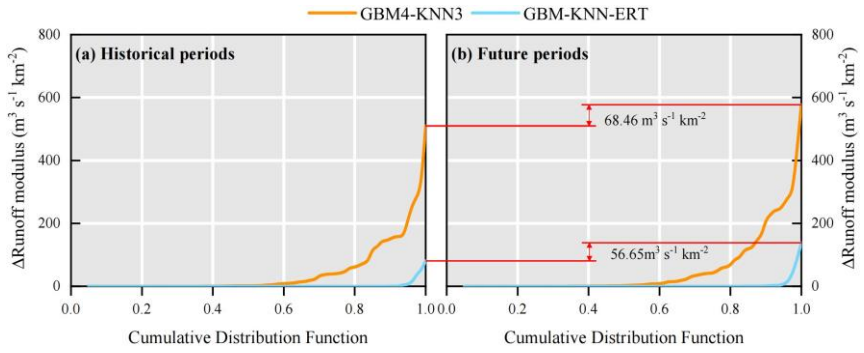

Fig.12. Comparison of flood peak runoff modulus between parameter regionalization and calibrated Top-SSF model results, showing cumulative distribution functions (CDFs) of absolute differences for 80 catchments during (a) historical and (b) future periods.

5.5. Uncertainty and limitation

The uncertainty in this study arises from several sources, including the hydrological model, the regionalization methods, and the data itself. A critical evaluation of these sources helps to contextualize our findings and assess the generalizability of the ensemble method. Uncertainty from the hydrological model is inherent in its structure and the calibrated parameters. Although the Top-SSF model performed well, its parameters are effective values subject to equifinality. This uncertainty in the true parameter values can be viewed as a form of calibration bias, which serves as the target data for our regionalization. To mitigate this, we employed the robust SCE-UA optimization algorithm and focused only on sensitive parameters. Uncertainty is also introduced by the regionalization methods themselves, as the training data derived from donor catchments are susceptible to errors that can impact model performance (Mosavi et al., 2018; Xu et al., 2021).

A specific methodological choice was the exclusion of deep learning architectures, such as Multilayer Perceptrons or Long Short-Term Memory (LSTM) networks. This

decision was guided by several factors. First, parameter regionalization is a static regression problem, mapping time-invariant catchment descriptors to model parameters, which does not align with the sequential data structure for which LSTM is designed. Second, deep networks typically require large datasets to avoid overfitting; with a dataset of 80 catchments, traditional machine learning methods like GBM and ERT are often more robust and less prone to memorizing training data. Third, a key advantage of parameter regionalization is its potential for physical interpretability. Unlike DL models, whose internal decision-making processes are often obscured within abstract weight matrices, the ensemble methods employed here offer more accessible transparency. The tree-based models (GBM and ERT) allow for the direct assessment of feature importance, enabling the verification of physical consistency. Furthermore, the KNN component provides instance-based interpretability by explicitly identifying the specific donor catchments used for transfer. This preserves the traceable logic of hydrological similarity, clearly indicating the geographical or physical source of the transferred parameters, which may be crucial for building the trust of the method in the water management of mountainous catchments.

批注 [L2]: Comment#2

Furthermore, the primary contribution of this study is not the identification of a single superior algorithm, but the demonstration of a data-driven framework for constructing a locally optimal ensemble. The complementarity of the chosen models was not assumed but empirically validated through a competitive evaluation process. Each of the seven machine learning methods was independently trained and assessed for its ability to estimate each sensitive parameter. The final GBM-KNN-ERT ensemble

was constructed by selecting only the empirically best-performing model for each parameter based on objective metrics (R^2, RMSE, STD). The very fact that different methods were selected for different hydrological parameters provides direct empirical evidence of their complementary strengths, thus validating the ensemble method.

Furthermore, the specific GBM-KNN-ERT ensemble identified is necessarily data-dependent, raising questions about its transferability. However, this study primary contribution is not the specific model combination itself, but rather the demonstration of a data-driven method for constructing a locally optimal ensemble. This method is designed to be generalizable; applying the same competitive evaluation process to a new region would identify the best ensemble for that specific dataset. The key to overcoming these limitations and ensuring robust generalization lies in genuine model complementarity. The ensemble method's success is not an artifact of overfitting to calibration bias or data quirks. Instead, it stems from a synergistic integration, where different models are empirically shown to be better suited for regionalizing parameters governed by distinct physical processes. The ensemble method's superior stability in the out-of-sample climate change stress test further supports this conclusion, indicating that it has captured robust underlying relationships, not just noise.

To manage methodological uncertainty, K-fold cross-validation was employed to ensure robust performance evaluation, and RandomizedSearchCV was used for hyperparameter tuning to minimize overfitting (Bergstra and Bengio, 2012). A key methodological decision was to evaluate the regionalization methods against the outputs of the calibrated Top-SSF model, rather than directly against observed flood

events. This approach was chosen for two primary reasons. First, it isolates the performance of the parameter regionalization itself. The calibrated simulation represents the theoretical upper bound of performance for the given hydrological model structure; consequently, any deviation from this benchmark can be directly attributed to imperfections in the regionalization method, rather than being confounded by the inherent structural limitations of the Top-SSF model. Second, this strategy ensures that the machine learning models learn the underlying physical relationships intended by the hydrological model, not simply mimic data noise or measurement errors present in the observations. If trained against raw observations, the machine learning methods might derive spurious parameter sets that compensate for both the hydrological model's structural flaws and observational errors. Such parameters could appear effective but would lack physical meaning and generalizability. These measures, combined with the evidence for model complementarity, provide a strong basis for the scientific validity and potential for generalization of our proposed ensemble method.

6. Conclusions

This study introduces a novel multi-machine learning ensemble method (GBM-KNN-ERT) to enhance model parameter transferability and improve flood prediction in ungauged mountainous catchments. The proposed GBM-KNN-ERT method demonstrated a substantial advancement in both flood prediction accuracy and model robustness, achieving exceptional performance with 90% of ungauged catchments exhibiting a NSE exceeding 0.9, a significant 67.44% improvement compared to the best single machine learning method evaluated in this study. Importantly, the GBM-

KNN-ERT method exhibited remarkable stability under simulated climate change, thereby highlighting its potential for reliable application in non-stationary hydrological environments. Furthermore, the method demonstrated notable adaptability to varying donor-catchment configurations, where an optimal balance between predictive accuracy and computational efficiency with a relatively limited set of 20–40 high-quality donor catchments (NSE >0.85). By integrating the diverse strengths of multiple machine learning with hydrological model, the proposed methodology significantly advances the field of flood prediction in ungauged catchments, offering a reliable tool for water resource management and flood disaster mitigation.

Acknowledgements

This research was supported by the Joint Funds of the National Natural Science Foundation of China (**U2240226**), the National Natural Science Foundation of China (**42271038**) and the National Key Research and Development Program of China (**2022FY100205**).

Competing interests

The authors declare that they have no known competing financial interests or personal relationships that could have appeared to influence the work reported in this paper.

Author contributions

In this study, K L, G W, and J G were responsible for the conceptualization of the research. Data curation was carried out by K L, L G, and X S, while formal analysis was performed by K L, J G, and J M. The methodology was developed by K L, L G, P

H, and J L. Project administration was overseen by G W and J G. K L took the lead in writing the original draft, and the writing, review, and editing process involved contributions from K L, G W, J L, P H, J M, X Z, and J G.

Code and data availability

The code used in this study is available upon request from the authors. The meteorological, soil characteristics, and topography datasets are publicly accessible online, as detailed in Table 1. The hourly flood data for the 80 catchments were sourced from China's Hydrological Yearbook. These data are not publicly available due to governmental restrictions but can be accessed by contacting the corresponding author for further information.

References

Arsenault, R., Breton-Dufour, M., Poulin, A., Dallaire, G.Romero-Lopez, R. (2019). Streamflow prediction in ungauged basins: analysis of regionalization methods in a hydrologically heterogeneous region of Mexico. Hydrological Sciences Journal, 64(11): 1297-1311. https://doi.org/10.1080/02626667.2019.1639716

Arsenault, R., Martel, J., Mai, J. (2022). Continuous streamflow prediction in ungauged basins: Long Short-Term Memory Neural Networks clearly outperform hydrological models. Hydrol. Earth Syst. Sci: 1-29. https://doi.org/10.5194/hess-27-139-2023

Bellman, R.E. (1961). On the reduction of dimensionality for classes of dynamic programming processes. RAND Corp., Santa Monica, Calif., Paper P-2243.

Bergstra, J.Bengio, Y. (2012). Random search for hyper-parameter optimization. Journal of machine learning research, 13(2).

Beven, K.J., Kirkby, M.J., Freer, J.E., Lamb, R. (2021). A history of TOPMODEL. Hydrology and Earth System Sciences, 25(2): 527-549. https://doi.org/10.5194/hess-25-527-2021S

Bishop, C.M.Nasrabadi, N.M., (2006). Pattern recognition and machine learning (information science and statistics). New York: Springer‐Verlag.

Breiman, L. (2001). Random forests. Machine learning, 45: 5-32.

Cheng, Q., Gao, L., Zuo, X.Zhong, F. (2019). Statistical analyses of spatial and temporal variabilities in total, daytime, and nighttime precipitation indices and of extreme dry/wet association with large-scale circulations of Southwest China,

795 1961–2016. Atmospheric research, 219: 166-182.
796 https://doi.org/10.1109/ACCESS.2018.2886549
797 Choi, J., Kim, U.Kim, S. (2023). Ecohydrologic model with satellite-based data for
798 predicting streamflow in ungauged basins. Science of The Total Environment,
799 903: 166617. https://doi.org/10.1016/j.scitotenv.2023.166617
800 Dai, Y., Shangguan, W., Duan, Q., Liu, B., Fu, S.Niu, G. (2013). Development of a
801 China dataset of soil hydraulic parameters using pedotransfer functions for land
802 surface modeling. Journal of Hydrometeorology, 14(3): 869-887.
803 https://doi.org/10.1175/JHM-D-12-0149.1
804 Dakhlaoui, H., Bargaoui, Z.Bárdossy, A. (2012). Toward a more efficient calibration
805 schema for HBV rainfall–runoff model. Journal of Hydrology, 444: 161-179.
806 https://doi.org/10.1016/j.jhydrol.2012.04.015
807 Ding, Y.Peng, S. (2020). Spatiotemporal trends and attribution of drought across China
808 from 1901–2100. Sustainability, 12(2): 477.
809 https://doi.org/10.3390/su12020477
810 Duan, Q., Sorooshian, S.Gupta, V.K. (1994). Optimal use of the SCE-UA global
811 optimization method for calibrating watershed models. Journal of Hydrology,
812 158(3): 265-284. https://doi.org/10.1016/0022-1694(94)90057-4
813 Friedman, J.H. (2002). Stochastic gradient boosting. Computational statistics & data
814 analysis, 38(4): 367-378. https://doi.org/10.1016/S0167-9473(01)00065-2
815 Gan, B., Liu, X., Yang, X., Wang, X.Zhou, J. (2018). The impact of human activities on
816 the occurrence of mountain flood hazards: lessons from the 17 August 2015
817 flash flood/debris flow event in Xuyong County, south-western China.
818 Geomatics, Natural Hazards and Risk, 9(1): 816-840.
819 https://doi.org/10.1080/19475705.2018.1480539
820 Gao, J., Kirkby, M.Holden, J. (2018). The effect of interactions between rainfall
821 patterns and land-cover change on flood peaks in upland peatlands. Journal of
822 Hydrology, 567: 546-559. https://doi.org/10.1016/j.jhydrol.2018.10.039
823 Garambois, P.A., Roux, H., Larnier, K., Labat, D.Dartus, D. (2015). Parameter
824 regionalization for a process-oriented distributed model dedicated to flash
825 floods. Journal of Hydrology, 525: 383-399.
826 https://doi.org/10.1016/j.jhydrol.2015.03.052
827 Gauch, M., Mai, J.Lin, J. (2021). The proper care and feeding of CAMELS: How
828 limited training data affects streamflow prediction. Environmental Modelling &
829 Software, 135: 104926. https://doi.org/10.1016/j.envsoft.2020.104926
830 Geurts, P., Ernst, D.Wehenkel, L. (2006). Extremely randomized trees. Machine
831 Learning, 63(1): 3-42. https://doi.org/10.1007/s10994-006-6226-1
832 Golian, S., Murphy, C.Meresa, H. (2021). Regionalization of hydrological models for
833 flow estimation in ungauged catchments in Ireland. Journal of Hydrology:
834 Regional Studies, 36: 100859. https://doi.org/10.1016/j.ejrh.2021.100859
835 Guo, L., Huang, K., Wang, G.Lin, S. (2022). Development and evaluation of
836 temperature-induced variable source area runoff generation model. Journal of
837 Hydrology, 610: 127894. https://doi.org/10.1016/j.jhydrol.2022.127894

838 Guo, Y., Zhang, Y., Zhang, L.Wang, Z. (2021). Regionalization of hydrological
839 modeling for predicting streamflow in ungauged catchments: A comprehensive
840 review. Wiley Interdisciplinary Reviews: Water, 8(1): e1487.
841 https://doi.org/10.1002/wat2.1487
842 Gupta, A.K., Chakroborty, S., Ghosh, S.K.Ganguly, S. (2023). A machine learning
843 model for multi-class classification of quenched and partitioned steel
844 microstructure type by the k-nearest neighbor algorithm. Computational
845 Materials Science, 228: 112321.
846 https://doi.org/10.1016/j.commatsci.2023.112321
847 Hastie, T., Tibshirani, R.Friedman, J., (2009). The elements of statistical learning.
848 Citeseer.
849 Hersbach, H., Bell, B., Berrisford, P., Biavati, G., Horányi, A., Muñoz Sabater, J.,
850 Nicolas, J., Peubey, C., Radu, R., Rozum, I., Schepers, D., Simmons, A., Soci,
851 C., Dee, D.Thépaut, J.-N., (2023). ERA5 hourly data on single levels from 1940
852 to present, Copernicus Climate Change Service (C3S) Climate Data Store
853 (CDS)[Dataset]. https://doi.org/10.24381/cds.adbb2d47 (Accessed on 08-06-
854 2023)
855 Hua, F., Wang, L., Fisher, B., Zheng, X., Wang, X., Douglas, W.Y., Tang, Y., Zhu,
856 J.Wilcove, D.S. (2018). Tree plantations displacing native forests: The nature
857 and drivers of apparent forest recovery on former croplands in Southwestern
858 China from 2000 to 2015. Biological Conservation, 222: 113-124.
859 https://doi.org/10.1016/j.biocon.2018.03.034
860 Jordan, M.I.Mitchell, T.M. (2015). Machine learning: Trends, perspectives, and
861 prospects. Science, 349(6245): 255-260. https://doi.org/10.1126/science.aaa841
862 Jung, Y. (2018). Multiple predicting K-fold cross-validation for model selection.
863 Journal of Nonparametric Statistics, 30(1): 197-215.
864 https://doi.org/10.1080/10485252.2017.1404598
865 Kanishka, G.Eldho, T. (2017). Watershed classification using isomap technique and
866 hydrometeorological attributes. Journal of Hydrologic Engineering, 22(10):
867 04017040. https://doi.org/10.1061/(ASCE)HE.1943-5584.0001562
868 Kratzert, F., Klotz, D., Herrnegger, M., Sampson, A.K., Hochreiter, S.Nearing, G.S.
869 (2019). Toward improved predictions in ungauged basins: Exploiting the power
870 of machine learning. Water Resources Research, 55(12): 11344-11354.
871 https://doi.org/10.1029/2019WR026065
872 Lenhart, T., Eckhardt, K., Fohrer, N.Frede, H.G. (2002). Comparison of two different
873 approaches of sensitivity analysis. Physics and Chemistry of the Earth, Parts
874 A/B/C, 27(9): 645-654. https://doi.org/10.1016/S1474-7065(02)00049-9
875 Li, K., Wang, G., Gao, J., Guo, L., Li, J.Guan, M. (2024). The rainfall threshold of
876 forest cover for regulating extreme floods in mountainous catchments. Catena,
877 236: 107707. https://doi.org/10.1016/j.catena.2023.107707
878 Li, X., Khandelwal, A., Jia, X., Cutler, K., Ghosh, R., Renganathan, A., Xu, S., Tayal,
879 K., Nieber, J.Duffy, C. (2022). Regionalization in a global hydrologic deep
880 learning model: from physical descriptors to random vectors. Water Resources
881 Research, 58(8): e2021WR031794. https://doi.org/10.1029/2021WR031794

Li, Z., Xu, X., Yu, B., Xu, C., Liu, M.Wang, K. (2016). Quantifying the impacts of climate and human activities on water and sediment discharge in a karst region of southwest China. Journal of Hydrology, 542: 836-849. https://doi.org/10.1016/j.jhydrol.2016.09.049

Liu, C., Guo, L., Ye, L., Zhang, S., Zhao, Y.Song, T. (2018). A review of advances in China's flash flood early-warning system. Natural hazards, 92: 619-634. https://doi.org/10.1007/s11069-018-3173-7

Luo, P., He, B., Takara, K., Xiong, Y.E., Nover, D., Duan, W.Fukushi, K. (2015). Historical assessment of Chinese and Japanese flood management policies and implications for managing future floods. Environmental Science & Policy, 48: 265-277. https://doi.org/10.1016/j.envsci.2014.12.015

McMillan, H.K. (2021). A review of hydrologic signatures and their applications. Wiley Interdisciplinary Reviews: Water, 8(1): e1499. https://doi.org/10.1002/wat2.1499

Morel-Seytoux, H.J.Khanji, J. (1974). Derivation of an equation of infiltration. Water Resources Research, 10(4): 795-800. https://doi.org/10.1029/WR010i004p00795

Mosavi, A., Ozturk, P.Chau, K.w. (2018). Flood prediction using machine learning models: Literature review. Water, 10(11): 1536. https://doi.org/10.3390/w10111536

Nearing, G., Cohen, D., Dube, V., Gauch, M., Gilon, O., Harrigan, S., Hassidim, A., Klotz, D., Kratzert, F., Metzger, A., Nevo, S., Pappenberger, F., Prudhomme, C., Shalev, G., Shenzis, S., Tekalign, T.Y., Weitzner, D.Matias, Y. (2024). Global prediction of extreme floods in ungauged watersheds. Nature, 627(8004): 559-563. https://doi.org/10.1038/s41586-024-07145-1

Pachauri, R.K., Allen, M.R., Barros, V.R., Broome, J., Cramer, W., Christ, R., Church, J.A., Clarke, L., Dahe, Q.Dasgupta, P., (2014). Climate change 2014: synthesis report. Contribution of Working Groups I, II and III to the fifth assessment report of the Intergovernmental Panel on Climate Change.

Papageorgaki, I.Nalbantis, I. (2016). Classification of Drainage Basins Based on Readily Available Information. Water Resources Management, 30(15): 5559-5574. https://doi.org/10.1007/s11269-016-1410-y

Pugliese, A., Persiano, S., Bagli, S., Mazzoli, P., Parajka, J., Arheimer, B., Capell, R., Montanari, A., Blöschl, G.Castellarin, A. (2018). A geostatistical data-assimilation technique for enhancing macro-scale rainfall–runoff simulations. Hydrology and Earth System Sciences, 22(9): 4633-4648. https://doi.org/10.5194/hess-22-4633-2018

Qi, W., Zhang, C., Fu, G.Zhou, H. (2016). Quantifying dynamic sensitivity of optimization algorithm parameters to improve hydrological model calibration. Journal of Hydrology, 533: 213-223. https://doi.org/10.1016/j.jhydrol.2015.11.052

Ragettli, S., Zhou, J., Wang, H., Liu, C.Guo, L. (2017). Modeling flash floods in ungauged mountain catchments of China: A decision tree learning approach for

parameter regionalization. Journal of Hydrology, 555: 330-346. https://doi.org/10.1016/j.jhydrol.2017.10.031

Rockström, J., Gupta, J., Qin, D., Lade, S.J., Abrams, J.F., Andersen, L.S., Armstrong McKay, D.I., Bai, X., Bala, G., Bunn, S.E., Ciobanu, D., DeClerck, F., Ebi, K., Gifford, L., Gordon, C., Hasan, S., Kanie, N., Lenton, T.M., Loriani, S., Liverman, D.M., Mohamed, A., Nakicenovic, N., Obura, D., Ospina, D., Prodani, K., Rammelt, C., Sakschewski, B., Scholtens, J., Stewart-Koster, B., Tharammal, T., van Vuuren, D., Verburg, P.H., Winkelmann, R., Zimm, C., Bennett, E.M., Bringezu, S., Broadgate, W., Green, P.A., Huang, L., Jacobson, L., Ndehedehe, C., Pedde, S., Rocha, J., Scheffer, M., Schulte-Uebbing, L., de Vries, W., Xiao, C., Xu, C., Xu, X., Zafra-Calvo, N.Zhang, X. (2023). Safe and just Earth system boundaries. Nature, 619(7968): 102-111. https://doi.org/10.1038/s41586-023-06083-8

Sain, S.R. (1996). The Nature of Statistical Learning Theory. Technometrics, 38(4): 409-409. https://doi.org/10.1080/00401706.1996.10484565

Salmeron, R., García, C.García, J. (2018). Variance inflation factor and condition number in multiple linear regression. Journal of statistical computation and simulation, 88(12): 2365-2384. https://doi.org/10.1080/00949655.2018.1463376

Schoups, G., van de Giesen, N.C.Savenije, H.H.G. (2008). Model complexity control for hydrologic prediction. Water Resources Research, 44(12). https://doi.org/10.1029/2008WR006836

Shangguan, W., Dai, Y., Liu, B., Zhu, A., Duan, Q., Wu, L., Ji, D., Ye, A., Yuan, H.Zhang, Q. (2013). A China data set of soil properties for land surface modeling. Journal of Advances in Modeling Earth Systems, 5(2): 212-224. https://doi.org/10.1002/jame.20026

Song, Z., Xia, J., Wang, G., She, D., Hu, C.Hong, S. (2022). Regionalization of hydrological model parameters using gradient boosting machine. Hydrology and Earth System Sciences, 26(2): 505-524. https://doi.org/10.5194/hess-26-505-2022

Tang, S., Sun, F., Liu, W., Wang, H., Feng, Y.Li, Z. (2023). Optimal Postprocessing Strategies With LSTM for Global Streamflow Prediction in Ungauged Basins. Water Resources Research, 59(7): e2022WR034352. https://doi.org/10.1029/2022WR034352

Wainwright, J.Mulligan, M., (2013). Environmental modelling: finding simplicity in complexity. John Wiley & Sons.

Wani, O., Beckers, J.V.L., Weerts, A.H.Solomatine, D.P. (2017). Residual uncertainty estimation using instance-based learning with applications to hydrologic forecasting. Hydrol. Earth Syst. Sci., 21(8): 4021-4036. https://doi.org/10.5194/hess-21-4021-2017

Wu, H., Zhang, J., Bao, Z., Wang, G., Wang, W., Yang, Y.Wang, J. (2022). Runoff modeling in ungauged catchments using machine learning algorithm-based model parameters regionalization methodology. Engineering. https://doi.org/10.1016/j.eng.2021.12.014

969 Xu, Q., Chen, J., Peart, M.R., Ng, C.-N., Hau, B.C.H.Law, W.W.Y. (2018). Exploration
970 of severities of rainfall and runoff extremes in ungauged catchments: A case
971 study of Lai Chi Wo in Hong Kong, China. Science of The Total Environment,
972 634: 640-649. https://doi.org/10.1016/j.scitotenv.2018.04.024
973 Xu, T.Liang, F. (2021). Machine learning for hydrologic sciences: An introductory
974 overview. Wiley Interdisciplinary Reviews: Water, 8(5).
975 https://doi.org/10.1002/wat2.1533
976 Yang, X., Magnusson, J., Rizzi, J.Xu, C.-Y. (2018). Runoff prediction in ungauged
977 catchments in Norway: comparison of regionalization approaches. Hydrology
978 Research, 49(2): 487-505. https://doi.org/10.2166/nh.2017.071
979 Yang, X., Magnusson, J.Xu, C.Y. (2019). Transferability of regionalization methods
980 under changing climate. Journal of Hydrology, 568: 67-81.
981 https://doi.org/10.1016/j.jhydrol.2018.10.030
982 Zhai, X., Guo, L., Liu, R.Zhang, Y. (2018). Rainfall threshold determination for flash
983 flood warning in mountainous catchments with consideration of antecedent soil
984 moisture and rainfall pattern. Natural Hazards, 94: 605-625.
985 https://doi.org/10.1007/s11069-018-3404-y
986 Zhang, B., Ouyang, C., Cui, P., Xu, Q., Wang, D., Zhang, F., Li, Z., Fan, L., Lovati, M.,
987 Liu, Y.Zhang, Q. (2024). Deep learning for cross-region streamflow and flood
988 forecasting at a global scale. The Innovation, 5(3).
989 https://doi.org/10.1016/j.xinn.2024.100617
990 Zhang, Y., Chiew, F.H., Li, M.Post, D. (2018). Predicting runoff signatures using
991 regression and hydrological modeling approaches. Water Resources Research,
992 54(10): 7859-7878. https://doi.org/10.1029/2018WR023325
993 Zhang, Y., Chiew, F.H., Liu, C., Tang, Q., Xia, J., Tian, J., Kong, D.Li, C. (2020). Can
994 remotely sensed actual evapotranspiration facilitate hydrological prediction in
995 ungauged regions without runoff calibration? Water Resources Research, 56(1):
996 e2019WR026236. https://doi.org/10.1029/2019WR026236
997 Zhang, Y., Ragettli, S., Molnar, P., Fink, O.Peleg, N. (2022). Generalization of an
998 Encoder-Decoder LSTM model for flood prediction in ungauged catchments.
999 Journal of Hydrology, 614: 128577.
1000 https://doi.org/10.1016/j.jhydrol.2022.128577
1001 Zounemat-Kermani, M., Batelaan, O., Fadaee, M.Hinkelmann, R. (2021). Ensemble
1002 machine learning paradigms in hydrology: A review. Journal of Hydrology, 598:
1003 126266. https://doi.org/10.1016/j.jhydrol.2021.126266

1004